

Electrostatically tuned rate of peptide self-assembly resolved by multiple particle tracking^{†‡}

Thierry Savin and Patrick S. Doyle*

Received 11th January 2007, Accepted 24th May 2007
First published as an Advance Article on the web 24th July 2007
DOI: 10.1039/b700434f

Hydrogels formed from the self-assembly of oligopeptides are being extensively studied for biomedical applications. The kinetics of their gelation, as well as a quantitative description of the forces controlling the rate of assembly has not yet been addressed. We report here the use of multiple particle tracking to measure the self-assembly kinetics of the model peptide FKFEFKFE (KFE8). KFE8 forms well-defined β -sheet intermediates and is often used as a model peptide system that forms a fibrous network in aqueous solvent. We find that increasing the pH of this system from 3.5 to 4.0 decreases the time of KFE8 gelation by almost hundredfold, from hours to minutes. A remarkable self-similarity between measurements performed at different pH suggests that, although accelerated by the pH increase, gelation follows an invariable mechanism. We propose a semi-quantitative interpretation for the order of magnitudes of gelation time using a simple model for the interaction driving the self-assembly in terms of the Derjaguin–Landau–Verwey–Overbeek (DLVO) theory. Such understanding is important for the development of current and future therapeutic applications (*e.g.* drug delivery).

1 Introduction

New synthetic biological materials formed by the self-assembly of designed peptides have shown considerable potential for biomedical applications. Notably, successful functional tissue recovery was recently observed by locally injecting solutions of these peptides into brain and heart lesions.^{1,2} In these studies, the authors used ionic self-complementary oligopeptides that form β -sheet structures through a hierarchical self-assembly, ultimately resulting in a fibrous network.^{3–6} The latter then served as a scaffold allowing cells' re-growth.^{7,8} A fundamental property of these materials for biomedical applications is the rapid sol–gel mechanical transition they undergo when immersed in physiological conditions.

The peptide called KFE8 (two repeats of the sequence FKFE, see the molecular structure given in Fig. S1 of the ESI[†]), is one of the simplest self-assembling peptides that forms fibrous matrices. Consequently this design, or very similar ones, has been extensively studied as a model system.^{4–6,9–12} KFE8 self-assembles into a helical bilayer of β -sheet intermediates, with hydrophobic side chains between the two layers^{5,6} (see Fig. S1 in the ESI[†] for an illustration of this molecular arrangement). Additionally, these fibers share many features with the amyloid fibrils found in protein-conformational diseases, and are thus also used as model systems to study the formation of amyloids.¹²

We asked ourselves what drives the self-assembly of the model system KFE8, and how fast it occurs. The mechanism by which these peptides coalesce to form a network is not clearly understood, but it is known that self-assembly is sensitive to the pH and the ionic strength of the solution, due to the ionizable side chains. Caplan *et al.*^{4,10,11} tentatively explained this dependence in terms of the Derjaguin–Landau–Verwey–Overbeek (DLVO) theory. They hypothesized that self-assembly of KFE12 (three repeats of FKFE) is promoted by the hydrophobic effect,¹³ but hindered by electrostatic repulsion of the charge-like faces of the molecule. When the molecule carries zero net charge, or when the charges are screened, self-assembly of fibers occurs extremely rapidly (seconds or less). On the other hand when the molecules are charged, self-assembly is slower (few hours or more). However the studies by Caplan *et al.* related the effect of relieving electrostatic peptide repulsion only to the late equilibrium state of the formed gel, through a binary sol–gel rheological assessment. Other studies were focused on early time intermediate structures' formation.^{5,6,12} In particular, molecular dynamics simulations have shown that the hydrophobic contacts precede the growth of backbone hydrogen bonds.¹²

The kinetics of the network formation can be partly resolved using circular dichroism (CD) spectroscopy.⁵ These measurements reported a steady increase in β -sheet structures and a concurrent decrease in the presence of coils. However, the knowledge of how these fibers interact and contribute progressively to the formation of a solid network cannot be assessed with CD spectroscopy. Here we use multiple particle tracking (MPT) microrheology to follow the hydrogel formation of the KFE8 self-assembling peptide.¹⁴ Intermediate states of the evolving system most likely contain fragile structures, that will either be disrupted by bulk rheometry, or have a rheological signature below the detection limit of a standard

Massachusetts Institute of Technology, Department of Chemical Engineering, 77 Massachusetts Avenue, Room 66-270, Cambridge, Massachusetts, 02139, USA. E-mail: pdoyle@mit.edu; Fax: +1 617-258-5042; Tel: +1 617-253-4534

† Electronic supplementary information (ESI) available: molecular model of peptide, peptide solution titration, peptide interaction in the crossed cylinders geometry. See DOI: 10.1039/b700434f

‡ MPT, multiple particle tracking; MSD, mean-squared displacement; TFA, trifluoroacetic acid

rheometer. In this regard, microrheometry is well suited to report accurate measurements on weak forming gels, without breaking their structural components.^{15,16} Another advantage of MPT microrheology is that measurements are fast (\sim minutes or less) and that the state of the sample, contained in a closed chamber, is not effected by external factors (e.g. evaporation). This characteristic is in dramatic contrast with bulk rheology, where measurements are usually longer, and elaborate sample preparation techniques are needed to circumvent evaporation.⁴ In this study, MPT allows us to show in particular that although the KFE8 self-assembly rate is dramatically tuned from hours to minutes by the variation of peptide net charge at different pH, the mechanism of gelation remains unchanged.

2 Results

2.1 Monitoring the kinetics of self-assembly

The lyophilized powder of peptide KFE8 was mixed in deionized filtered water to a concentration of 0.1 wt% (1 mg ml⁻¹), and microspheres were added to the solution. Due to residual trifluoroacetic acid (TFA) from peptide synthesis, the pH of the solution was \sim 3.3. We adjusted the pH by adding NaOH into the solution to reach a concentration [NaOH]₀ that we chose from a titration of the peptide-powder solution (see the titration curve, Fig. S2 in the ESI†). We then performed a time series of MPT measurements as the self-assembly was occurring in the observed sample of KFE8 solution. For each

time point during the gelation, we calculated the one-dimensional ensemble averaged mean-squared displacement (MSD) $\langle \Delta x^2(\tau) \rangle$ as a function of the lag time τ to quantify the dynamics of the embedded Brownian probes. We report the results of this computation in Fig. 1A corresponding to amine-coated beads of 1 μm diameter, in a solution of 0.1 wt% KFE8 crude powder at pH = 3.5 ([NaOH]₀ = 0.65 mM). The times of gelation explored range from 3 min to 5 days. At the beginning of the gelation, when no gel network has been formed in the sample, the dynamics of the particles are the ones obtained in a purely viscous fluid ($\langle \Delta x^2(\tau) \rangle \propto \tau$, as indicated by the dash-dotted line in Fig. 1A). This initial viscosity can be evaluated from the slope of $\langle \Delta x^2(\tau) \rangle = 2D\tau$ using the expression of the self-diffusion coefficient $D = k_B T/(6\pi a\eta)$, where k_B is the Boltzmann's constant, T the absolute temperature ($T = 23$ °C in all our experiments), η the viscosity of the fluid and a the particle radius. We find $\eta = 2$ mPa s, that is about twice the viscosity of water, at this early time of gelation. As the self-assembly occurs, the MSD continuously decreases since the motion of the probes is progressively more constrained by the formation of fibers in their surrounding. At long times of gelation when the equilibrium state of the peptide system is reached (see further discussions later in the text), the MSD is almost a constant plateau ($\langle \Delta x^2(\tau) \rangle = \langle \Delta x_p^2 \rangle$ independent of τ) indicating that the fluid behaves as an elastic material at the frequencies measured here, from 0.1 to 10 Hz. At this point, the elastic modulus G is evaluated using $G = 2k_B T/(6\pi a\langle \Delta x_p^2 \rangle)$. We find $G = 1$ Pa, indicating the presence of a weak gel with

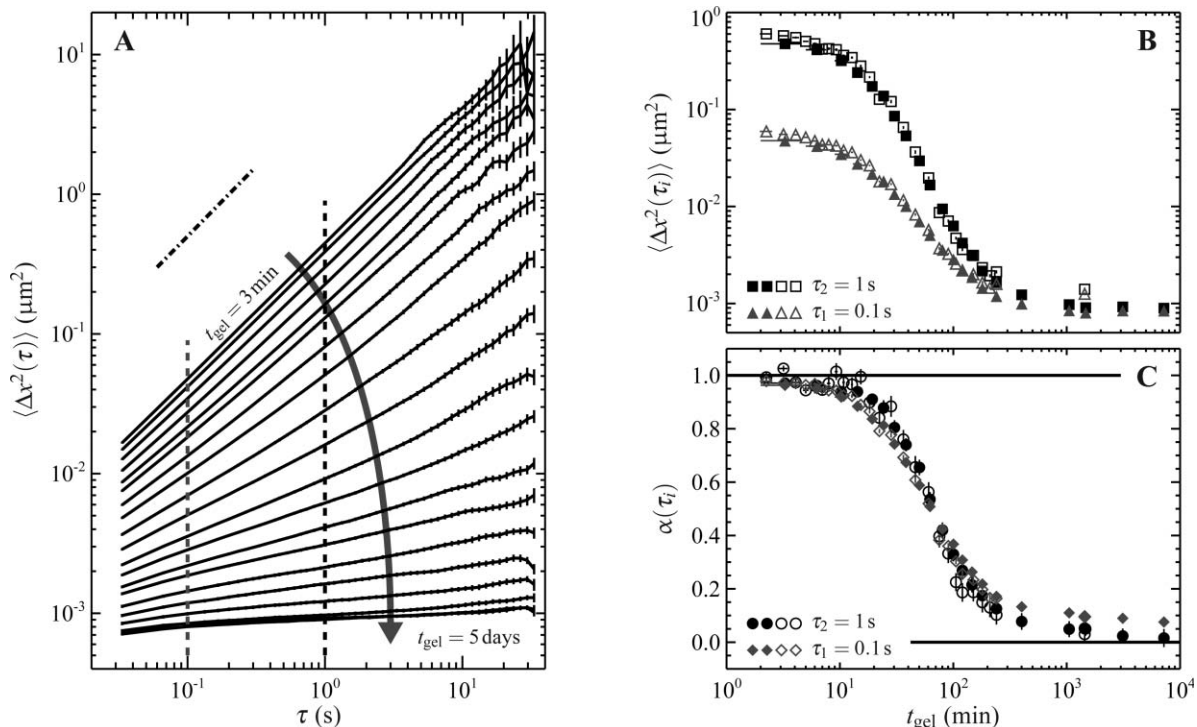


Fig. 1 Ensemble averaged MSD $\langle \Delta x^2(\tau) \rangle$ of probes (1 μm diameter, amine-coated) embedded in the self-assembling KFE8 system, reported at different times during gelation, from 3 min to 120 h. The concentration of peptide powder is 0.1 wt%, and the pH of the solution was set to 3.5. (A) The variation of $\langle \Delta x^2(\tau) \rangle$ versus τ for different times of gelation t_{gel} . The dash-dotted line indicates the scaling $\langle \Delta x^2(\tau) \rangle \propto \tau$. (B) $\langle \Delta x^2(\tau_i) \rangle$ at two lag times $\tau_i = 0.1$ (triangles) and 1 s (squares), versus t_{gel} . The solid symbols are extracted from (A) (at values of τ shown in (A) by the dashed lines). (C) The value of the local power-law $\alpha(\tau_i)$ versus t_{gel} at the same two lag times than (B), $\tau_i = 0.1$ (diamonds) and 1 s (circles). The solid lines in (C) indicate the limiting values 0 and 1 for $\alpha(\tau)$. In (B) and (C), the open symbols are a reproducibility check.

the same elasticity to that found using bulk rheology on a similar system at comparable concentration.¹⁷

To follow the kinetics, it is convenient to represent the evolution of the MSD, evaluated at a given lag time, with the self-assembly progression.¹⁸ In Fig. 1B we plot the quantity $\langle \Delta x^2(\tau_i) \rangle$, calculated at two lag times $\tau_1 = 0.1$ s and $\tau_2 = 1$ s, as a function of the time of gelation t_{gel} . Also, in Fig. 1C we show the variation of the local power-law $\alpha(\tau_i)$ calculated at the same two lag times as a function of t_{gel} . The local power-law, or diffusive exponent, is defined by:

$$\alpha(\tau) = \frac{d(\log \langle \Delta x^2(\tau) \rangle)}{d(\log \tau)} \quad (1)$$

We observe on these plots that both the MSD $\langle \Delta x^2(\tau_i) \rangle$ and the diffusive exponent $\alpha(\tau_i)$ remain constant for gelation times greater than 1000 min, suggesting that the system has reached an equilibrium state. This time scale is consistent with the characteristic kinetics of structure formation apparent on the AFM micrographs measured by Marini *et al.*⁵ These latter experiments were performed at a lower pH (~ 3.3), meaning that the gel-formation kinetics are expected to be slower (see section 2.3). However, we can presume from the figures in ref. 5 that the gel has reached an equilibrium state at a time between 2 and 30 h.

Also, we observe on the curves presented in Fig. 1C that the local power-law values are independent of the lag time at which they are calculated, for any point in time during gelation. By looking at the MSD in Fig. 1A, we notice indeed that for all t_{gel} , $\langle \Delta x^2(\tau) \rangle$ exhibits a pure power-law dependence with τ over almost the entire range of accessible lag times. As noticed earlier, this power-law varies from 1 at the beginning of the self-assembly, indicating a purely viscous behavior, and reaches almost 0 at the equilibrium state of the gel, characteristic of a purely elastic behavior on the accessible range of frequencies.

We have validated our experimental protocol by reproducing these kinetics data under identical conditions in a separate experiment (*c.f.* open symbols in Fig. 1B and 1C). We observe good reproducibility, in terms of both the amplitude of $\langle \Delta x^2(\tau) \rangle$ and $\alpha(\tau)$ at various lag times, and also in their evolution with t_{gel} . However, we note that the last point of $\langle \Delta x^2(\tau) \rangle$ at $t_{\text{gel}} = 1500$ min, characterizing the equilibrium state, differs by about 40% between the two experiments, indicating the sensitivity of this final state of the system to small variations, beyond control, in the experimental conditions.

2.2 Probes' surface chemistry and size

Ideally, the measurement technique should not interfere with the self-assembly mechanism of gelation. Here, the probe particles could exhibit unwanted interaction with the assembly process. To characterize the effect of surface chemistry and size of the probe particles, we performed the experiment described above with another surface coating of the probes and a different size. First, we applied MPT on 0.925 μm diameter carboxylate-modified probes in a solution of KFE8 powder at a concentration of 0.1 wt% with pH set at 3.5 (same as in the previous section). At this pH, carboxylate-modified probes are negatively charged whereas the amine-modified particles are positively charged. The peptide in solution at this pH being

itself positively charged (see inset of Fig. 5 and later in the text), we evaluate here the influence of a possible interaction between the bead and the peptide. Moreover, this comparison is performed with similar particle sizes, so we truly isolate the effect of surface chemistry. We present in Fig. 2 the kinetics results at the lag time $\tau_2 = 1$ s using these two different surface chemistries. Note that the MSD values reported in Fig. 2A are scaled by the probe radius a . We observe in this plot that the MSD of the carboxylated particles (negatively charged) is, in general, smaller than the one exhibited by the amine-coated particles (positively charged). This trend is consistent with other microrheological studies comparing the response of probes strongly and weakly attracted to their surrounding network.¹⁹ We can hypothesize for example that the carboxylated beads are attached to the fibers through electrostatic attraction, connecting meshes and limiting locally the network fluctuations and hence their own motion. We used 1 μm diameter amine-modified probes in section 2.3 to eventually limit these sorts of weak interactions with peptide

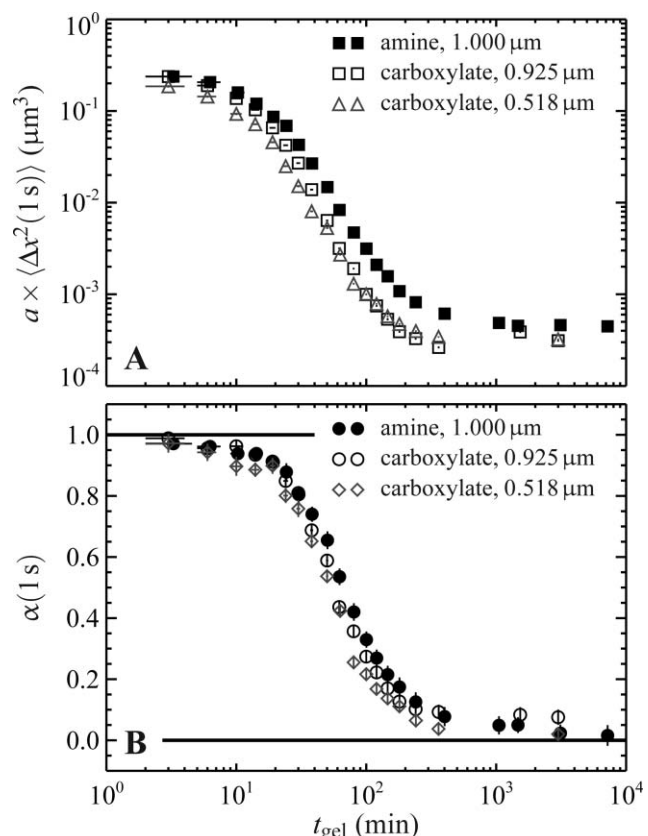


Fig. 2 Scaled MSD $a \times \langle \Delta x^2(\tau) \rangle$ and local power-law $\alpha(\tau)$ for particles of different surface chemistries and sizes, embedded in the self-assembling KFE8 system as a function of self-assembly time t_{gel} . The concentration of powder is 0.1 wt%, and the pH of the solution was set to 3.5. The lag time is $\tau = 1$ s. (A) The filled squares correspond to 1 μm diameter amine-coated probes, the open squares are for 0.925 μm diameter carboxylate-modified probes, and the triangles are for 0.518 μm diameter carboxylate-modified particles. (B) The filled circles are for 1 μm diameter amine-coated probes, whereas the open symbols are for 0.925 μm (circles) 0.518 μm (diamonds) diameter carboxylate-modified probes. The solid black lines in (B) indicates the limiting values 0 and 1 for $\alpha(\tau)$.

self-assembly. At the beginning of self-assembly, however, the scaled values are identical in the absence of a formed network. The amplitude of the difference between the MSDs obtained at long gelation times with these two chemistries is nevertheless small (the equilibrium values for $\langle \Delta x^2(1\text{ s}) \rangle$ with carboxylate-modified probes are about 50% lower than with amine-coated probes, a discrepancy comparable to the one obtained in the reproducibility test mentioned previously), and the local power-law as shown in Fig. 2B are almost identical at all times of gelation.

We next performed a kinetics study using 0.518 μm diameter carboxylate-modified probes, and the results are also presented in Fig. 2. We observe that the scaled MSDs for these smaller beads, as well as the local power-law they exhibit, are collapsing onto the data for the bigger beads with the same carboxylate surface chemistry. The independence of the quantity $a \times \langle \Delta x^2(\tau) \rangle$ with the probe radius suggests that the particles are probing a continuum environment at the lengths scale of their diameter (at least for $a > 0.5\text{ }\mu\text{m}$). Note that this is consistent with estimates of the averaged mesh size of a KFE8 system at similar concentration, calculated from AFM micrographs or electron micrographs of similar systems at comparable concentrations.⁷ Also the aforementioned similitude in the dynamics of probes bound and non-bound to the fiber matrix corroborates the idea of a continuous network at the length scale of the probe.

These findings suggest that bulk rheometry can be extracted from the ensemble-averaged MSD using the generalized Stokes–Einstein relation.²⁰ We show in Fig. 3 the resulting rheological data obtained from the MSD. The storage and loss modulus, respectively $G'(\omega)$ and $G''(\omega)$, were calculated at the frequency ω using $G^*(\omega) = G'(\omega) + iG''(\omega)$ with:

$$G^*(\omega) \approx \frac{k_B T}{3\pi a} \frac{\exp[i\pi\alpha(1/\omega)/2]}{\langle \Delta x^2(1/\omega) \rangle \Gamma[1+\alpha(1/\omega)]} \quad (2)$$

where Γ is the gamma function, as described in ref. 21 and 22. We observe the qualitative behavior described in the previous

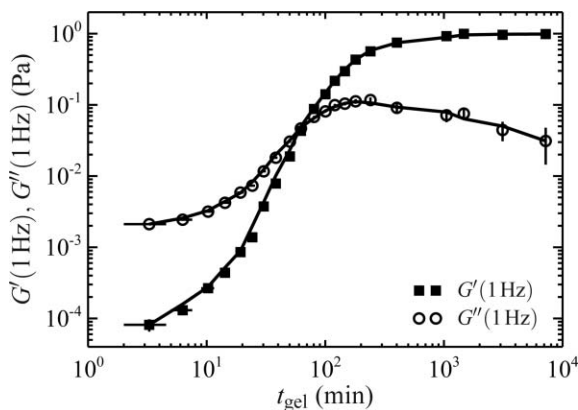


Fig. 3 Evolution of the storage modulus $G'(\omega)$ (solid squares) and of the loss modulus $G''(\omega)$ (open circles) as a function of the self-assembly time for a KFE8 powder solution with concentration of 0.1 wt% and a pH of 3.5. The values $G'(\omega)$ and $G''(\omega)$ were calculated from the ensemble averaged MSD of 1 μm diameter amine-modified particles at a frequency $\omega = 1\text{ Hz}$. Changing the size and/or the surface chemistry of the probe particles does not significantly affect these results.

section, that is the material is almost purely viscous at the beginning of the self-assembly, and its storage modulus progressively increases to become larger than the loss modulus, meaning that the material is essentially elastic at long times. At time $t_{\text{gel}} > 1000\text{ min}$, the gel's rheological properties remain steady.

2.3 Characteristic time of self-assembly

In order to quantify the influence of the pH on the kinetics of gelation, we must define a characteristic time of self-assembly that we can evaluate from the MPT measurements. The critical gel point t_{gel}^0 of the sol–gel transition of a gelling system is the first instant at which the connectivity of the network extends over the entire sample. At the time t_{gel}^0 , the longest relaxation time of the critical gel diverges and a power-law behavior is observed for both $G'(\omega) \propto \omega^{\alpha_0}$ and $G''(\omega) \propto \omega^{\alpha_0}$ over a wide range of frequencies.²³ This power-law dependency is presumably related to the fractal scaling properties of the network clusters.²⁴

In our study we have access to a frequency range spanning two decades, $0.1\text{ Hz} < \omega < 10\text{ Hz}$, with good statistical accuracy (see Fig. 1A). Over this range we observe that the MSD exhibits a power-law behavior $\langle \Delta x^2(\tau) \rangle \propto \tau^\alpha$ at all times of gelation. Application of the generalized Stokes–Einstein relation shows that in this case, both $G'(\omega) \propto \omega^\alpha$ and $G''(\omega) \propto \omega^\alpha$ over the corresponding range of frequencies. It is likely however that the system exhibits some relaxation dynamics whose characteristic times lie outside this range, at a certain time of self-assembly before and after the gel point. However, given the frequency window available here, the gel point cannot be determined using solely the power-law criteria mentioned above. Nevertheless we can postulate a characteristic value for α_0 to determine the critical gel time. Using dynamic scaling based on percolation theory with the Rouse limit of hydrodynamic interactions, ones find $0.5 < \alpha_0 < 0.66$.^{25–27} The latter Rouse dynamics model with $\alpha_0 = 0.5$ has been successful in describing rheology near the gel point.^{25,28} Such criteria allows the definition of the gel point (t_{gel}^0 , $G'_0 = G''_0$) which in that case corresponds to the gelation time at which the curves for G' and G'' cross each other, as seen in Fig. 3.

In Fig. 4 we present the results for the gel-point time as a function of the pH for a KFE8 powder solution with a concentration of 0.1 wt%. We performed these MPT measurements using 1 μm diameter amine-coated probes, and with a concentration of $[\text{NaOH}]_0$ between 0.65 and 1 mM. The values of t_{gel}^0 for each pH reported in Fig. 4B were extracted from the evolution of the local power-law α with the gelation time (as presented in Fig. 4A) by using the criteria $\alpha = \alpha_0 = 0.5$ to define the gel point. We observe that the self-assembly is faster as the pH increases. For an elevation of pH from 3.5 to 4, the gel time is decreased by almost two orders of magnitude, from $\sim 70\text{ min}$ to $\sim 1\text{ min}$. The amplitude of this variation is fairly independent of the choice of α_0 for the gel-point criteria in the viscoelastic region $0.2 < \alpha_0 < 0.8$, meaning that another choice of α_0 in this range would lead to values of t_{gel}^0 scaled by the same constant factor for all values of pH as compared to the one in Fig. 4B.

We also report in Fig. 4B the evolution of the characteristic elastic modulus $G'_0 = G''_0$ at the gel point characterized by the crossover between the elastic and viscous behavior. We

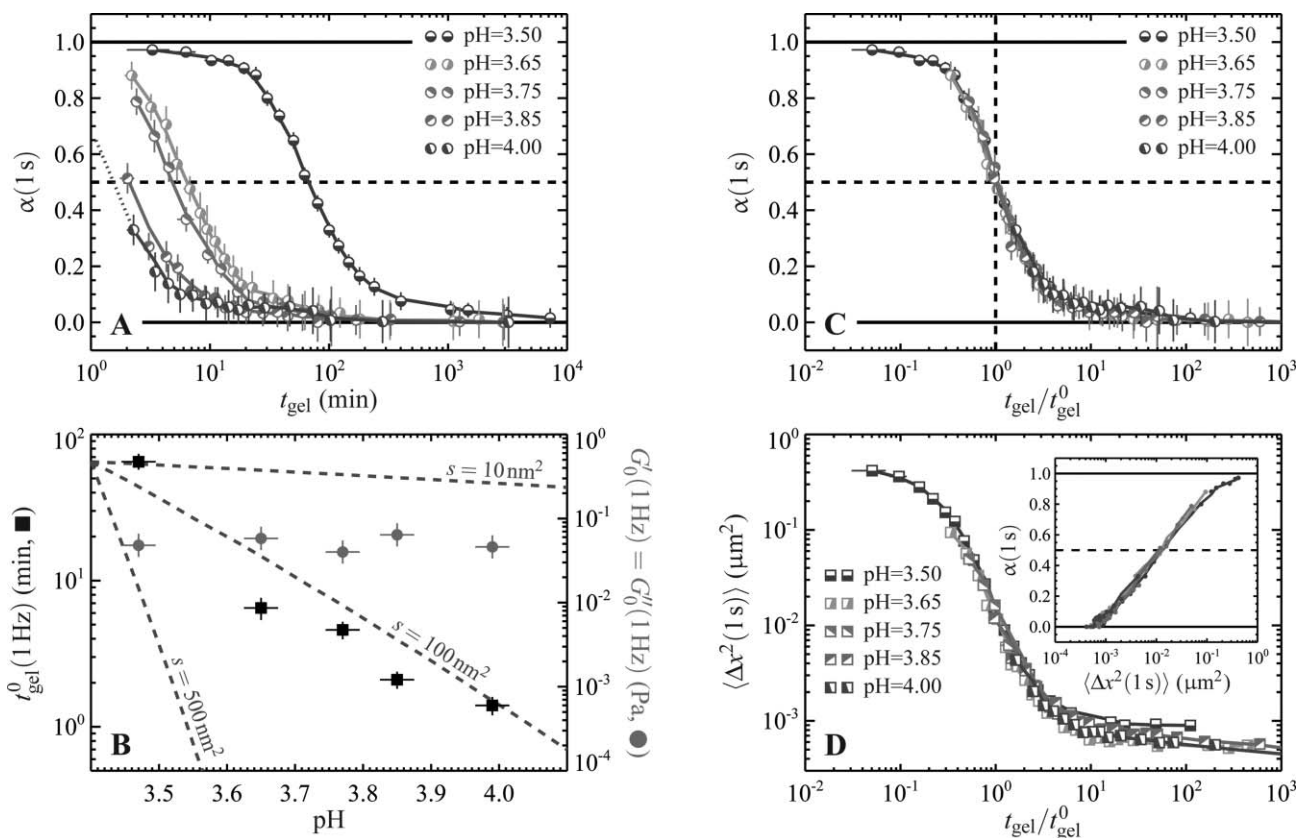


Fig. 4 Gelation kinetics of KFE8 powder solution with concentration 0.1 wt% as a function of the pH. (A) The local power-law of the MSD at a lag time $\tau = 1$ s, plotted as a function of the gelation time t_{gel} for pH = 3.5, 3.65, 3.75, 3.85 and 4 (see legend on the figure). The critical gel point t_{gel}^0 is uniquely obtained at $\alpha = \alpha_0 = 0.5$, as represented by the dashed line. (B) The resulting t_{gel}^0 (squares) and $G'_0 = G''_0$ (circles) as a function of the pH. The range of modulus reported here (10^{-4} to 1 Pa) is the same as the range displayed in Fig. 3. The dashed lines are W_{pH} versus pH for the three values of s indicated (see section 3.2.3, the prefactor is arbitrary chosen to fall in the range shown here). (C) The same results as presented in (A) (the same symbols are used to distinguish the pH), but the gelation time t_{gel} has been scaled by the gel-point time t_{gel}^0 obtained at the corresponding pH for each curve. (D) The value of the MSD as a function of the gelation time scaled the same way as in (C). The inset in (D) shows the evolution of the local power-law versus the magnitude of the MSD. All the quantities presented here are evaluated at $\tau = 1$ s and $\omega = 1$ Hz.

observe that even though the kinetics are dramatically changed by the increase of pH, the mechanical properties are not significantly affected by the pH at the gel point. This observation suggests that in this range of pH the self-assembling peptide, as probed by particle tracking at the gel point, passes through an identical mechanical state independent of the pH. We can extend this observation by presenting the kinetics measurements scaled by the characteristic gel time t_{gel}^0 extracted from Fig. 4A. In Fig. 4C and 4D we present the evolution of $\alpha(1\text{ s})$ and $\langle\Delta x^2(1\text{ s})\rangle$, respectively, as a function of $t_{\text{gel}}/t_{\text{gel}}^0$ for each value of pH. We observe a remarkable overlap of these curves. The scatter of the points at late gelation time, $t_{\text{gel}}/t_{\text{gel}}^0 > 10$ is within the reproducibility control presented in Fig. 1 for the equilibrium state. This self-similarity strongly suggests that the increase of the pH from 3.5 to 4.0 does not affect the mechanism by which peptides self-assemble, but merely increases the rate. This observation will be the basis of the gelation model presented in the next section. The inset of Fig. 4D summarizes this self-similarity in the observable parameter space ($\alpha, \langle\Delta x^2\rangle$) at a lag time $\tau = 1$ s, but the same result holds for other lag times investigated in this study (data not shown).

3 Discussion

In this section, we propose interpretations of the trends observed experimentally by using simplified and semi-quantitative models, that nevertheless capture the expected physics of the phenomena. Simplifications in these models allow us to reduce the range of adjustable parameters to solely geometric considerations. First, we question if the initial viscosity of the peptide solution can be explained by the presence of the early non-connected structures that were directly observed in previous studies.⁵ Second, we suggest a model of the interaction driving the self-assembly that accounts for the observed characteristic gelation times.

3.1 Peptides' structure at early state

We measured the viscosity of the peptide KFE8 solution at the beginning of gelation for a pH of 3.5, and we found it to be twice the viscosity of the aqueous solvent in which the peptide powder is mixed. From the direct observations of peptides' early state structure,^{5,29} we assume that, at short gelation times (t_{gel}), the KFE8 mixture is a monodisperse solution of peptide ribbons that we model as cylinders with radius $R = 3.5$ nm (see

Fig. S1 in the ESI†) and length L that can be related to n , the number of peptide molecules per ribbon segment. One turn of the helix contains about 100 KFE8 molecules and is about 20 nm long,⁶ and so $L = n \times 0.2$ nm. We use $v = n^{-1} \times 4 \times 10^{23}$ m⁻³ for the number density of rods in solution (as obtained with 80% purity of a 0.1 wt% KFE8 powder dissolved in the solvent, see the titration model presented in the ESI†). The transition from a dilute to a semi-dilute regime for a dispersion of such cylinders occurs when v is greater than $v^* = L^{-3}$. In our case, we calculate that this transition occurs when fibers are longer than $L^* \approx 100$ nm, which is the typical size of initial ribbons reported in ref. 5. This indicates that the dispersion is expected to be between the dilute and semi-dilute regime. The zero-shear rate viscosity of a dispersion of Brownian rods in this intermediate regime can be written in terms of the rotational diffusion coefficient D_r of the rods:³⁰

$$\eta \approx \eta_0 + \frac{vk_B T}{30D_{r,0}} + \frac{vk_B T}{10D_r} \quad (3)$$

where η and η_0 are the dispersion and solvent viscosities respectively, and $D_{r,0}$ is the limit of D_r at infinite dilution (in this limit, the above expression becomes $\eta \approx \eta_0 + 2vk_B T/(15D_{r,0})$ for the dilute regime). An accurate expression of the rotational friction coefficient $\zeta_r = k_B T/D_{r,0}$ for long cylinders can be found in ref. 31 and 32:

$$\zeta_r = \frac{k_B T}{D_{r,0}} = \frac{\pi \eta_0 L^3}{3 \ln \lambda} f(\ln \lambda) \quad \text{with} \quad f(x) = \frac{x+0.64}{x-1.5} + \frac{1.659}{x^2} \quad (4)$$

where $\lambda = L/R$ is the aspect ratio of the cylinder. An expression for $D_{r,0}$ can be calculated from the above equation. Using a tube model, Doi and Edwards estimated $D_r = \beta D_{r,0}(vL^3)^{-2}$, where β is a numerical constant equal to about 1000.³⁰ Combining the above equations, we finally obtain the intrinsic viscosity of the dispersion:

$$[\eta] = \frac{\eta - \eta_0}{\phi \eta_0} \approx \frac{\lambda^2 f(\ln \lambda)}{90 \ln \lambda} + \frac{\lambda^6 f(\ln \lambda)}{30 \pi^2 \beta \ln \lambda} \phi^2 \quad (5)$$

in terms of the volume fraction $\phi = \pi R^2 L v = 0.3\%$. Solving eqn (5) for L with $(\eta - \eta_0)/\eta_0 = 1$, we find $L \approx 500$ nm, corresponding to earlier ribbons of about 25 helical turns long. Note that we can count about 10 helical turns per precursor ribbon on the AFM micrograph obtained in ref. 5 with the same concentration of peptide powder, after 8 min of self-assembly (although the peptide-powder mixing protocol was significantly shorter), and at a pH ≈ 3.3. With this value of L we calculate $v/v^* \approx 30$, which usually indicates the transition from dilute to semi-dilute behavior,³² thus confirming the use of eqn (3). The model above neglects the contribution of the electrostatic repulsion between the charged rods. However in the semi-dilute regime, this interaction merely results in increasing L , the characteristic size of the excluded volume effect, to an effective length of rods that incorporates the range of the electrostatic repulsion, $L + \kappa^{-1}$ (where κ^{-1} is the Debye length, see next section).³³ This range of $\kappa^{-1} \approx 10$ nm, as evaluated later in the text, is much smaller than the physical length $L \approx 500$ nm. Thus the effect of charges on eqn (5) can be neglected. Moreover for such high aspect ratio objects (here

$\lambda \approx 150$), the drag coefficient is weakly dependent on the fine geometry of the body,³¹ thus allowing us to model the helical fibers (whose pitch is 20 nm, much smaller than L) by simple cylinders.

3.2 Self-assembly rate tuned by electrostatic double layer interactions

We must assume a geometric scenario for the elementary coalescence of initial peptide structures in order to model the interaction driving the self-assembly of KFE8. In a simplified model, we assume that the β-sheet formed by the peptides is a semi-infinite block with a given surface s of interaction by which two identical blocks could eventually connect. This geometry has already been used on the same system by Hwang *et al.*⁶ to develop their model of peptide-surface charge in terms of the electrostatic double layer theory. We assume that the early short fibers are somewhat represented by these blocks of material. Though this choice might not be the most advanced, the resulting theory remains, however, fairly simple, and allows us to calculate reasonable orders of magnitude for the interaction. An alternate scenario for the geometry of the interaction is investigated in the ESI†.

3.2.1 Modeling the peptide charge. In the electrostatic double layer model, the charged blocks are bathed in a solution of ions. To calculate the total surface-charge density σ and the electrostatic potential ψ_s at the surface of the blocks, Hwang *et al.*⁶ used the local chemical equilibrium condition of the β-sheet in the solution.¹³ They found:

$$\frac{\tilde{\sigma}}{\tilde{\sigma}_{\max}} = - \frac{10^{pH - pK_E}}{e^{-\tilde{\psi}_s} + 10^{pH - pK_E}} + \frac{e^{-\tilde{\psi}_s}}{e^{-\tilde{\psi}_s} + 10^{pH - pK_K}} \quad (6)$$

where $\tilde{\sigma} = e\sigma/(\epsilon k_B T)$ is the scaled surface-charge density, and $\tilde{\psi}_s = e\psi_s/(k_B T)$ is the scaled potential at the block's surface. In our notations, e is the elementary electric charge and $\epsilon = \epsilon_r \epsilon_0$ with ϵ_r and ϵ_0 being the dielectric constant of water (~ 80) and the permittivity of vacuum, respectively. The Debye-Hückel parameter, written $\kappa = \sqrt{2e^2 ce^{-1}/(k_B T)}$, is a function of the ion concentration $c = [\text{OH}^-] + [\text{T}^-]$ that itself depends on the pH through $c = 10^{pH - 14} + [\text{T}]_0(1 + 10^{pK_T - pH})^{-1}$, where $[\text{T}]_0$ and $pK_T = 0.52$ are the initial concentration and dissociation pK value of TFA, respectively. Also in eqn (6), $pK_E = 4.3$ and $pK_K = 10.8$ are the dissociation pK constants of the glutamic acid EH and of the Lysine KH⁺, respectively (since the model presented here is local, these surface dissociation pK constants are the standard values of the isolated amino acids^{34,35}). The quantity $\sigma_{\max} = 0.26$ C m⁻² is the maximum possible surface charge of the block, as calculated from the dimensions of the KFE8 molecule: two positive groups on an area 3.1×0.4 nm² exposed to the bulk (see Fig. S1 in the ESI†). In the electrostatic double layer model, the surface-charge density and the surface potential are also related by the Grahame equation, that is written in our case:^{6,13}

$$\tilde{\sigma} = 2 \sinh(\tilde{\psi}_s/2) \quad (7)$$

for the planar geometry, as obtained in a symmetrical 1 : 1 electrolyte with ion concentration c .

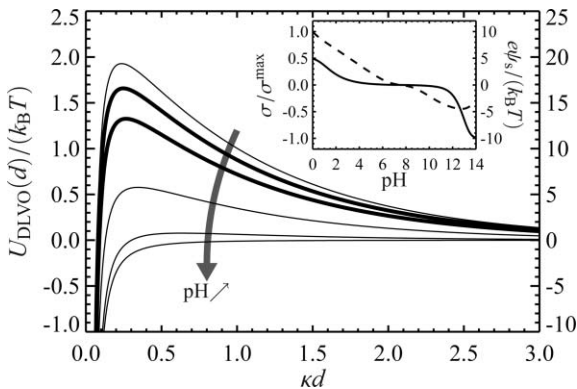


Fig. 5 DLVO interaction potential calculated from eqn (8) for pH = 3.5 and 4 (thick lines). The thin lines are for pH = 3, 5, 6 and 7, from the top to the bottom line. The left axis is for a characteristic surface of interaction $s = 10 \text{ nm}^2$, whereas the right axis is for $s = 100 \text{ nm}^2$. The inset gives the surface-charge density and electrostatic potential of the peptides for $[T]_0 = 10^{-3} \text{ M}$ as a function of the pH of the bath solution. The solid line represents the surface-charge density σ/σ_{\max} , and the dashed line is for the surface potential $\psi_s = e\psi_s/(k_B T)$. The window of pH observed in this study is $3.5 < \text{pH} < 4$.

Eqn (6) in conjunction with eqn (7), can be used to calculate σ and ψ_s at every pH. The results are given in the inset of Fig. 5 with a TFA concentration $[T]_0 = 10^{-3} \text{ M}$ (see the ESI†). We see that the peptide is positively charged for $\text{pH} \lesssim 4$ and negatively charged for $\text{pH} \gtrsim 11$. In these domains of pH, we expect that the electrostatic repulsion between the peptides slows down the self-assembly process. The bulk rheology measurements would conclude to a non-elastic state of the material unless the sample is assessed after a prohibitively long equilibration time. This observation is in agreement with the rheology results obtained by Caplan *et al.* with the peptide KFE12¹⁰ that would share a similar theoretical curve as the one presented in Fig. 5.

3.2.2 Interaction potential. We use a van der Waals interaction potential to describe the attractive component of the blocks' interaction. It is certain that many forces are driving the self-assembly. The hydrophobic bond is usually the dominant one, and it has been shown through simulations that it contributes to the short time association of peptides in the initial β -sheet.¹² The hydrogen bonds are likely to ensure the cohesion of the blocks, and are responsible for the peculiar helical shape of the β -sheet. The van der Waals dispersion forces are long range and are usually responsible for bringing the molecules together.^{13,36} Such a model has been used by Grigsby *et al.*³⁷ for poly-L-lysine peptide, in which they also included short-range specific interactions (*e.g.* hydrophobic bonds) that are discarded here.

The potential of net interaction of two blocks of material separated by a distance d and with a characteristic surface s of interaction is given by:¹³

$$\frac{U_{\text{DLVO}}(d)}{k_B T} = \frac{4sc}{\kappa} \Psi_s^2 e^{-kd} - \frac{sA}{12\pi d^2} \quad (8)$$

where A is the Hamaker constant, taken to be $A = 5k_B T$ for proteins in aqueous solutions.³⁸ The effective potential Ψ_s is given by $\Psi_s = 4\tanh(\tilde{\psi}_s/4)$.

The Debye length κ^{-1} (10 nm) is bigger than the typical radius (3.5 nm) of the cross-section of the KFE8 double-layer ribbon (see Fig. S1 in the ESI†). In Fig. 5 we plot the interaction potential given by eqn (8) in the planar geometry at various pH, and for $s = 10 \text{ nm}^2$ and $s = 100 \text{ nm}^2$ corresponding to dimensions of $\sim 3 \times 3 \text{ nm}$ and $\sim 10 \times 10 \text{ nm}$, respectively, for the surface of blocks' interaction. This last characteristic size of 10 nm is intended to include the electrostatic layer on the side of the β -sheet, and thus to account for edge effects in an admittedly *ad hoc*, but analytically tractable, manner.

We observe in Fig. 5 that the potential barrier value U_{DLVO}^{\max} is decreasing as the pH increases from 3 to 7, as expected from the corresponding decrease of the surface-charge density σ on the interacting blocks (see inset). At $\text{pH} > 6$, we observe that $U_{\text{DLVO}}^{\max} < k_B T$, meaning that the potential barrier is not significant and that the block monomers can easily assemble. In that case, the system is expected to quickly form a stable network, as seen experimentally.⁴

3.2.3 Time scales. From the interaction potential given above it is possible to extract some time scale of network growth using colloidal aggregation theories. The characteristic time to form dimers from interacting monomer can be written $t_{\text{DLVO}} = t_B \times W$, where $t_B = 3\eta_0/(4k_B T v)$ is the characteristic Brownian aggregation time for a diffusion limited process, and W is the Fuchs stability factor.³⁹ We have $t_B \approx n \times 10^{-7} \text{ s}$ (with $\eta_0 = 1 \text{ mPa s}$, and $v = n^{-1} \times 4 \times 10^{23} \text{ m}^{-3}$ as previously used) and

$$W = 2d_{\max} \int_{d_{\max}}^{\infty} e^{U_{\text{DLVO}}(x)/k_B T} \frac{dx}{x^2} \quad (9)$$

where d_{\max} is the distance between monomer at which the interaction potential $U_{\text{DLVO}}(x)$ is maximum.³⁹ Although these relations were derived for a spherical interacting monomer, we expect the time t_{DLVO} to be correlated to the gel-point time, t_{gel}^0 measured experimentally in this study. Indeed, we recall that t_{gel}^0 is the time at which the self-assembly first percolates the entire sample, and thus closely related to the dynamics of growth of the structuring element.

As observed in Fig. 4, t_{gel}^0 increases by a factor of 50 as the pH is reduced from 4 to 3.5. By assuming $t_{\text{DLVO}} \propto t_{\text{gel}}^0$, we thus expect to have $W_{\text{pH}=3.5}/W_{\text{pH}=4} \sim 50$. The integral in eqn (9) can be numerically evaluated using the expression of $U_{\text{DLVO}}(d)$ from eqn (8). We find $W_{\text{pH}=3.5}/W_{\text{pH}=4} = 1.3$ for $s = 10 \text{ nm}^2$, and $W_{\text{pH}=3.5}/W_{\text{pH}=4} = 30$ for $s = 100 \text{ nm}^2$. In Fig. 4B, the dashed lines show the influence of this free parameter on the expected magnitudes of the gelation time scales. For the surface of interaction $s = 100 \text{ nm}^2$ that matches the experimental results (see Fig. 4), we calculate $W_{\text{pH}=3.5} \approx 10^6$, which leads to $t_{\text{DLVO}} \approx n \times 0.1 \text{ s}$. If we take $n \approx 1000$, we obtain $t_{\text{DLVO}} \sim 1 \text{ min}$, which is the right order of magnitude for the system's gelation at this pH, assuming the concentration of monomer is negligible after $\sim 100 \times t_{\text{DLVO}}$, and that the gel point is reached at this instant.

An alternative model geometry in which self-assembly is controlled by an interaction between two crossed cylinders (tentatively representing the bundling of two fibers) is presented in the ESI†. This model however fails in describing

realistic time scales as compared to the experimental results. Although our findings seem to be more consistent with a gelation mechanism dominated by fiber growth rather than bundling, more detailed studies should be performed to elucidate this point. In particular, modeling the helical fibers by simple cylinders, as performed in the ESI†, is certainly a coarse approximation in our case, given the similitude between the helical pitch (20 nm) of the interacting object and the Debye length (10 nm).

In summary, we performed a novel assessment of the kinetics of peptide self-assembly. We found that a small change in the pH of the solution results in almost a hundred-fold variation of the gelation time, even at the low concentration of peptides used here. This high sensitivity to chemical conditions is an important property of these peptide-based materials, which is of high value in current biomedical applications such as tissue repair. We also observed a self-similarity in the measurements, suggesting that although the rate is greatly affected by the pH, the mechanism of gelation is independent of the pH. Knowing that a change of pH tunes the charges of the peptide, we investigated gelation times predicted by a simple model for electrostatically-mediated self-assembly of the peptides. The orders of magnitude for assembly time scales calculated with the DLVO model are remarkably realistic. The model can also be used to predict how the kinetics of gelation are tuned when changing the chemistry of the peptide solution. These predictions are likely to optimize the development of future applications such as drug delivery. More immediately, we anticipate that this study will guide the development of future numerical simulations and more advanced models that will help to provide a deeper understanding of the structural mechanism for peptide self-assembly.

4 Experimental

The peptide KFE8, of sequence [COCH₃]-FKFEFKFE-[CONH₂] was custom-synthesized from Synpep Corporation (Dublin, CA), and the lyophilized powder was stored at 4 °C. Solutions of 3 mg ml⁻¹ were obtained by thoroughly mixing the powder with deionized filtered water for 18 min using cycles of 1 min of vortexing and 5 min of sonicating to obtain a homogeneous solution. Immediately after mixing, the concentration of powder was reduced to 1 mg ml⁻¹ in a solution of fluorescent particles. The beads we used were amine-modified 1 μm diameter particle (Molecular Probes, Eugene, OR), and carboxylate-modified with diameters of 0.518 and 0.925 μm (Polysciences, Warrington, PA). The final volume fraction of fluorescent beads was such that $\phi \leq 0.05\%$. Also, this concentration of powder was chosen to match other previous studies.^{5,6} Vortexing for 1 min ensured the beads to be well dispersed in the solution. Finally, NaOH was added at the target concentration to increase the pH of the solution. When kinetics studies were performed, the initial time ($t_{\text{gel}} = 0$) was chosen at the moment of the addition of NaOH, that was followed by a final step of short vortexing of 30 s.

The sample was then rapidly loaded into a custom-made chamber for observation that was mounted on the microscope to immediately perform measurements. The particles' motion was observed at room temperature, $T = 23$ °C, with

a 40× objective (N.A. = 0.75) for the 1 and 0.925 μm diameter particles, and a 63× water-immersion objective (N.A. = 1.2) for the 0.518 μm particle. Movies of 1000 frames were recorded at a rate of 30 frames per seconds with an exposure time of 1 ms to reduce the dynamic errors.⁴⁰ The image processing algorithm developed by Crocker and Grier⁴¹ were applied to the de-interlaced movie to extract the one-dimensional trajectories of the multiple probes. The MSD values were calculated at various lag times using unbiased estimates derived in ref. 42. Static errors from camera noise were then corrected on the estimated MSD $\langle \Delta x^2(\tau) \rangle$ of the probes by following methods described by Savin and Doyle⁴³ to obtain a resolution $\sim 10^{-4}$ μm² in $\langle \Delta x^2(\tau) \rangle$.

Acknowledgements

We gratefully acknowledge Dr Wonmuk Hwang, Dr Davide Marini, Dr Roger Kamm and Dr Shuguang Zhang for insightful discussions. This material is based upon work supported by the National Science Foundation under Grant No. 0239012 (Career Award) and 0304128 (NSF-NIRT).

References

- 1 R. G. Ellis-Behnke, Y.-X. Liang, S.-W. You, D. K. C. Tay, S. Zhang, K.-F. So and G. E. Schneider, *Proc. Natl. Acad. Sci. U. S. A.*, 2006, **103**, 5054–5059.
- 2 M. E. Davis, J. M. Motion, D. A. Narmoneva, T. Takahashi, D. Hakuno, R. D. Kamm, S. Zhang and R. T. Lee, *Circulation*, 2005, **111**, 442–450.
- 3 S. Zhang, T. Holmes, C. Lockshin and A. Rich, *Proc. Natl. Acad. Sci. U. S. A.*, 1993, **90**, 3334–3338.
- 4 M. R. Caplan, P. N. Moore, S. Zhang, R. D. Kamm and D. A. Lauffenburger, *Biomacromolecules*, 2000, **1**, 627–631.
- 5 D. M. Marini, W. Hwang, D. A. Lauffenburger, S. Zhang and R. D. Kamm, *Nano Lett.*, 2002, **2**, 295–299.
- 6 W. Hwang, D. M. Marini, R. D. Kamm and S. Zhang, *J. Chem. Phys.*, 2003, **118**, 389–397.
- 7 T. C. Holmes, S. de Lacalle, X. Su, G. Liu, A. Rich and S. Zhang, *Proc. Natl. Acad. Sci. U. S. A.*, 2000, **97**, 6728–6733.
- 8 J. Kisiday, M. Jin, B. Kurz, H. Hung, C. Semino, S. Zhang and A. J. Grodzinsky, *Proc. Natl. Acad. Sci. U. S. A.*, 2002, **99**, 9996–10001.
- 9 E. J. Leon, N. Verma, S. Zhang, D. A. Lauffenburger and R. D. Kamm, *J. Biomater. Sci., Polym. Ed.*, 1998, **9**, 297–312.
- 10 M. R. Caplan, E. M. Schwartzfarb, S. Zhang, R. D. Kamm and D. A. Lauffenburger, *Biomaterials*, 2002, **23**, 219–227.
- 11 M. R. Caplan, E. M. Schwartzfarb, S. Zhang, R. D. Kamm and D. A. Lauffenburger, *J. Biomater. Sci., Polym. Ed.*, 2002, **13**, 225–236.
- 12 W. Hwang, S. Zhang, R. D. Kamm and M. Karplus, *Proc. Natl. Acad. Sci. U. S. A.*, 2004, **101**, 12916–12921.
- 13 J. N. Israelachvili, *Intermolecular and Surface Forces*, Academic Press, London, UK, 1985.
- 14 T. Savin and P. S. Doyle, *Bull. Am. Phys. Soc.*, 2004, **49**, 1014.
- 15 J. Apgar, Y. Tseng, E. Fedorov, M. B. Herwig, S. C. Almo and D. Wirtz, *Biophys. J.*, 2000, **79**, 1095–1106.
- 16 C. Veerman, K. Rajagopal, C. S. Palla, D. J. Pochan, J. P. Schneider and E. M. Furst, *Macromolecules*, 2006, **39**, 6608–6614.
- 17 A. P. Nowak, V. Breedveld, L. Pakstis, B. Ozbas, D. J. Pine, D. Pochan and T. J. Deming, *Nature*, 2002, **417**, 424–428.
- 18 Y. Tseng, K. M. An and D. Wirtz, *J. Biol. Chem.*, 2002, **277**, 18143–18150.
- 19 M. T. Valentine, Z. E. Perlman, M. L. Gardel, J. H. Shin, P. Matsudaira, T. J. Mitchison and D. A. Weitz, *Biophys. J.*, 2004, **86**, 4004–4014.
- 20 T. G. Mason and D. A. Weitz, *Phys. Rev. Lett.*, 1995, **74**, 1250–1253.

- 21 T. G. Mason, K. Ganesan, J. H. van Zanten, D. Wirtz and S. C. Kuo, *Phys. Rev. Lett.*, 1997, **79**, 3282–3285.
22 T. G. Mason, *Rheol. Acta*, 2000, **39**, 371–378.
23 H. H. Winter and M. Mours, *Adv. Polym. Sci.*, 1997, **134**, 165–234.
24 M. Muthukumar, *J. Chem. Phys.*, 1985, **83**, 3161–3168.
25 W. Hess, T. A. Vilgis and H. H. Winter, *Macromolecules*, 1988, **21**, 2536–2542.
26 J. E. Martin, D. Adolf and J. P. Wilcoxon, *Phys. Rev. Lett.*, 1988, **61**, 2620–2623.
27 M. Muthukumar, *Macromolecules*, 1989, **22**, 4656–4658.
28 H. H. Winter and F. Chambon, *J. Rheol.*, 1986, **30**, 367–382.
29 D. M. Marini, *Structure and Formation of β -sheet Fibers*, PhD thesis, Massachusetts Institute of Technology, 2003.
30 M. Doi and S. F. Edwards, *The Theory of Polymer Dynamics*, Oxford University Press, Oxford, UK, 1986.
31 G. K. Batchelor, *J. Fluid Mech.*, 1970, **44**, 419–440.
32 R. G. Larson, *The Structure and Rheology of Complex Fluids*, Oxford University Press, Oxford, UK, 1999.
33 A. M. Wierenga and A. P. Philipse, *Colloids Surf., A: Physicochem. Eng. Asp.*, 1998, **137**, 355–372.
34 L. Stryer, *Biochemistry*, W. H. Freeman and Company, New York, NY, 2000.
35 P. J. Kundrotas and A. Karshikoff, *Phys. Rev. E: Stat. Phys., Plasmas, Fluids, Relat. Interdiscip. Top.*, 2001, **65**, 011901.
36 D. Leckband and S. Sivasankar, *Colloids Surf., B: Biointerfaces*, 1999, **14**, 83–97.
37 J. J. Grigsby, H. W. Blanch and J. M. Prausnitz, *Biophys. Chem.*, 2002, **99**, 107–116.
38 S. Nir, *Prog. Surf. Sci.*, 1977, **8**, 1–58.
39 W. B. Russel, D. A. Saville and W. R. Schowalter, *Colloidal Dispersions*, Cambridge University Press, Cambridge, UK, 1989.
40 T. Savin and P. S. Doyle, *Phys. Rev. E: Stat. Phys., Plasmas, Fluids, Relat. Interdiscip. Top.*, 2005, **71**, 041106.
41 J. C. Crocker and D. G. Grier, *J. Colloid Interface Sci.*, 1996, **179**, 298–310.
42 T. Savin and P. S. Doyle, *Phys. Rev. E: Stat. Phys., Plasmas, Fluids, Relat. Interdiscip. Top.*, 2007.
43 T. Savin and P. S. Doyle, *Biophys. J.*, 2005, **88**, 623–638.



Comments received from just a few of the thousands of satisfied RSC authors and referees who have used ReSourCe - the online portal helping you through every step of the publication process.

authors benefit from a user-friendly electronic submission process, manuscript tracking facilities, online proof collection, free pdf reprints, and can review all aspects of their publishing history

referees can download articles, submit reports, monitor the outcome of reviewed manuscripts, and check and update their personal profile

NEW!! We have added a number of enhancements to ReSourCe, to improve your publishing experience even further.

New features include:

- the facility for authors to save manuscript submissions at key stages in the process (handy for those juggling a hectic research schedule)
- checklists and support notes (with useful hints, tips and reminders)
- and a fresh new look (so that you can more easily see what you have done and need to do next)

Go online today and find out more.

08030526

Registered Charity No. 207890

RSC Publishing

www.rsc.org/resource